Effect of Lag Damper Failure on Helicopter Ground Resonance

Jonah Whitt
Undergraduate Research Assistant

Farhan Gandhi
Redfern Professor and MOVE Director

Center for Mobility with Vertical Lift (MOVE)
Rensselaer Polytechnic Institute, Troy, New York

ABSTRACT

This paper examines ground resonance of a helicopter with a 4-bladed rotor with degradation in one of the lag dampers. The analysis is conducted with lag equations in individual blade coordinates solved using Floquet theory, lag equations in multi-blade coordinates solved using Floquet theory, and lag equations in multi-blade coordinates simplified using a constant coefficient approximation and then solved as an eigenvalue problem. From the study it was observed that regardless of whether the blade lag motions are in individual or multi-blade coordinates, the predicted stability levels are identical if the analysis is conducted using Floquet theory. In multi-blade coordinates, collective and differential lag needs to be retained in the analysis, unlike the case of a classical ground resonance analysis where only the cyclic lag modes and body motions are required. Using the constant coefficient approximation in multi-blade coordinates it is equivalent to smearing the damping loss of a single damper equally over all the damper. With the constant coefficient approximation predicts a smaller reduction in damping with damper degradation than the Floquet method, with the differences increasing as the level of degradation increases. For a completely failed damper, the loss in system damping predicted using the constant coefficient approximation was 46% of that from the Floquet analysis for an articulated rotor, and 55% for a hingeless rotor.

INTRODUCTION

It is well known that helicopters with articulated or soft in-plane hingeless/bearingless main rotors are susceptible to ground resonance instability when coalescence of the marginally damped rotor lead-lag and fuselage modes occurs (Refs. 1–3). The widely adopted solution to overcoming the ground resonance problem is through the introduction of auxiliary damping, with lead-lag dampers on the main rotor and landing gear dampers for fuselage mode damping. While other methods to improve aeromechanical stability have also been considered in the literature (e.g., use of rotor aeroelastic couplings, Refs. 4–9, active control, Refs. 10–13, or through tailoring the stiffness properties of the landing gear, Ref. 14), auxiliary dampers remain the most widely used solution. In using auxiliary dampers, the helicopter designer or OEM must ensure that the dampers are sized to alleviate ground resonance in all operating conditions, e.g., with change in aircraft gross weight, or ground contact conditions.

While the landing gear dampers undergo loading only when the aircraft is on the ground, the lead-lag dampers undergo periodic loading through the entire flight; thus accumulating many cycles over the course of their operating lives. In addition, the lead-lag dampers can also experience very large temperature variations, and large amplitude and multi-frequency excitations, putting them in harsh overall operating conditions. Yet, the effect of lead-lag damper degradation or failure on ground resonance has only been considered minimally in the literature (Ref. 15). The present study seeks to address this question, *and systematically examine the effect of degradation and failure in one of the lead-lag dampers on a helicopter's ground resonance stability*.

ANALYSIS

The present study considers a 4-bladed rotor (N=4), with the blades each undergoing rigid body in-plane rotations about their lag hinges. These lag motions, in the rotating system, can be described using individual blade coordinates: ζ_1, ζ_2, ζ_3 and ζ_4. Longitudinal and lateral translations of the rotor hub ($\bar{x}$ and $\bar{y}$) are also considered. The resulting combined system, with six degrees-of-freedom, is presented in Eq. 1. Aerodynamic forces, which are not a dominant factor in ground resonance, are neglected. It should be noted that with the lag motions represented using individual blade coordinates, the equations contain non-negligible periodic terms. Applying a constant coefficient approximation would be infeasible as it would entirely suppress the rotor-fuselage coupling (critical to the development of ground resonance), but the system's stability characteristics could be correctly

Presented at the Vertical Flight Society's 78th Annual Forum & Technology Display, Ft. Worth, TX, USA, May 10-12, 2022.

evaluated using Floquet Transition Matrix theory (Refs. 16, 2 and 3). In Eq. 1, Ω represents the rotational speed of the rotor, and the definition and values of the rotor-body parameters S_ζ^*, M_x^*, M_y^*, ω_x, ω_y and ν_ζ, which appear in standard ground resonance analyses, are provided in Table 1. The definition and values of system damping parameters ζ_x, ζ_y and C_ζ/I_ζ, are provided in Table 2. Specific to the present study, α_1 represents the degradation in blade 1 damper properties, with α_1=0 corresponding to no degradation whatsoever (completely healthy damper), α_1=1 corresponding to a completely failed damper, and intermediate values corresponding to varying levels of degradation.

Next, the coupled rotor-body equations are transformed to multi-blade coordinates, with ζ_o (collective lag), ζ_2 (differential lag), and ζ_{1c} and ζ_{1s} (cyclic lag degrees of freedom), in place of individual blade motions (ζ_1, ζ_2, ζ_3 and ζ_4). The coupled system, after transformation, is presented in Eq. 2, with the terms C11– C44 defined in Eq. 3, and the terms K13, K14, K23, K24, K33, K34, K43 and K44 defined in Eq. 4. It should be noted that when α_1=0 (no degradation or damage in damper 1), all the periodic terms in Eq. 2 disappear, and the collective and differential lag equations decouple from the rest of the system. This essentially returns the classical 4DOF (ζ_{1c}, ζ_{1s}, $\bar{x}$, $\bar{y}$) Coleman-Feingold constant coefficient system that can be solved as an eigenvalue problem to analyze ground resonance. With $\alpha_1 \neq 0$, the collective (ζ_o) and differential (ζ_2) lag equations do not decouple from the cyclic lag and body equations, and the periodic terms in the equation require the use of Floquet theory for stability analysis.

If the constant coefficient approximation is applied to Eq. 2, the terms in Eq. 3 and 4 simplify to those in Eq. 5 and 6. The collective and differential lag equations are coupled to each other (for $\alpha_1 \neq 0$), but are decoupled from the ζ_{1c}, ζ_{1s}, $\bar{x}$, $\bar{y}$ system. As it turns out, using the constant coefficient approximation is mathematically equivalent to smearing the loss of damping in damper 1 over the number of blades on the rotor, and in effect replacing C_ζ everywhere in the classical Coleman-Feingold equations by $C_\zeta\left(1-\frac{\alpha_1}{N}\right)$. Using the constant coefficient approximation after transforming to multi-blade coordinates allows for the solution of a simple eigenvalue problem instead of using Floquet theory for stability analysis, although it can be expected that there would be some error associated with the approximation (equivalent to smearing the loss in damping of a single damper equally over all the dampers).

This study considers both an articulated rotor with a non-dimensional rotating lag frequency of ν_ζ = 0.285/rev, and a soft in-plane hingeless rotor with a ν_ζ = 0.65/rev at a 300 RPM (5 Hz) nominal rotational speed. Using the above for rotor lag frequencies, the parameters in Table 1, and first setting rotor and body damping parameters (C_ζ, ζ_x and ζ_y) to zero, the modal frequencies and modal damping, in multi-blade coordinates, are shown in Figs. 1 and 2 for the articulated rotor and in Figs. 3 and 4 for the hingeless rotor. For the articulated rotor, the regressing lag mode coalesces with body-x mode between 2.2–3 Hz, and with body-y mode between 3.3–5 Hz. The damping of the coupled regressing lag and body modes goes negative over those ranges (implying the system suffers from ground resonance instability). Similarly, for the hingeless rotor, coalescence of the regressing lag mode with body-x and body-y modes is observed between 5–5.2 Hz and 5.8–6.6 Hz, respectively, and the system is again observed to be unstable over those ranges. The instability of the hingeless rotor is seen to be milder than the articulated rotor, as expected. By trial and error, a combination of fuselage and lag damping is determined that would completely stabilize the system and eliminate ground resonance. The values of damping parameters ζ_x, ζ_y and C_ζ/I_ζ, are provided in Table 2 for both the articulated and hingeless cases.

ARTICULATED ROTOR RESULTS AND DISCUSSION

Consider, first, an isolated rotor (with no body motion, $\bar{x}$= 0, $\bar{y}$=0) where the lag motion of the blades is represented using individual blade coordinates (ζ_1, ζ_2, ζ_3 and ζ_4). Eliminating the body degrees-of-freedom in Eq. 1 results in a constant coefficient system, and the modal frequencies and decay rates can be easily calculated by solving an eigenvalue problem. Figure 5 shows the modal frequencies, and Fig. 6 shows the decay rates for the healthy rotor, as well as with increasing degradation in damper 1. The modes are uncoupled and simply correspond to the motion of each individual blade, with the modal frequencies corresponding to the blade lag frequency in the rotating system ($\omega_\zeta = \sqrt{S_\zeta^* \bar{e}}\,\Omega$). In the absence of any damper degradation, the decay rate of all the modes (corresponding to the motion of the individual blades) are identical, as expected. When damper 1 is degraded ($\alpha_1 \neq 0$), the decay rates for three modes corresponding to motions of blades 2, 3, and 4, remain the same as the nominal, while the decay rate for the mode corresponding to motion of blade 1 decreases in proportion to the value of α_1. For α_1 = 1 (complete failure of damper 1), the decay rate for the mode corresponding to motion of blade 1 goes to zero.

Next, the stability characteristics are examined for the coupled rotor-body system with the lag motions still represented using individual blade coordinates (Eq. 1). The system has periodic coefficients and stability is examined using Floquet Transition Matrix theory. It is again noted that attempting to use a constant coefficient approximation would simply eliminate all rotor-body coupling, making it unsuitable for ground resonance analysis. Using Floquet Transition Matrix theory, Fig. 7 shows the minimum modal decay rate for increasing degradation levels of blade 1 damper (from α_1 = 0, healthy damper; to α_1 = 1, completely failed damper).

We consider next the system with the rotor lag motions represented in multi-blade coordinates (Eq. 2). First, the isolated rotor is considered (with no body motion, $\bar{x}$= 0, $\bar{y}$=0).

$$\begin{bmatrix} 1 & 0 & 0 & 0 & S_\zeta^*\sin(\psi) & -S_\zeta^*\cos(\psi) \\ 0 & 1 & 0 & 0 & S_\zeta^*\sin\left(\psi+\frac{\pi}{2}\right) & -S_\zeta^*\cos\left(\psi+\frac{\pi}{2}\right) \\ 0 & 0 & 1 & 0 & S_\zeta^*\sin(\psi+\pi) & -S_\zeta^*\cos(\psi+\pi) \\ 0 & 0 & 0 & 1 & S_\zeta^*\sin\left(\psi+\frac{3\pi}{2}\right) & -S_\zeta^*\cos\left(\psi+\frac{3\pi}{2}\right) \\ \frac{S_\zeta^*}{M_x^*N}\sin(\psi) & \frac{S_\zeta^*}{M_x^*N}\sin\left(\psi+\frac{\pi}{2}\right) & \frac{S_\zeta^*}{M_x^*N}\sin(\psi+\pi) & \frac{S_\zeta^*}{M_x^*N}\sin\left(\psi+\frac{3\pi}{2}\right) & 1 & 0 \\ -\frac{S_\zeta^*}{M_y^*N}\cos(\psi) & -\frac{S_\zeta^*}{M_y^*N}\cos\left(\psi+\frac{\pi}{2}\right) & -\frac{S_\zeta^*}{M_y^*N}\cos(\psi+\pi) & -\frac{S_\zeta^*}{M_y^*N}\cos\left(\psi+\frac{3\pi}{2}\right) & 0 & 1 \end{bmatrix} \begin{bmatrix} \overset{**}{\zeta_1} \\ \overset{**}{\zeta_2} \\ \overset{**}{\zeta_3} \\ \overset{**}{\zeta_4} \\ \overset{**}{\bar{x}_h} \\ \overset{**}{\bar{y}_h} \end{bmatrix}$$

+

$$\begin{bmatrix} \frac{\boldsymbol{C_\zeta}}{\boldsymbol{I_\zeta\Omega}}(\mathbf{1}-\boldsymbol{\alpha_1}) & 0 & 0 & 0 & 0 & 0 \\ 0 & \frac{C_\zeta}{I_\zeta\Omega} & 0 & 0 & 0 & 0 \\ 0 & 0 & \frac{C_\zeta}{I_\zeta\Omega} & 0 & 0 & 0 \\ 0 & 0 & 0 & \frac{C_\zeta}{I_\zeta\Omega} & 0 & 0 \\ 2\frac{S_\zeta^*}{M_x^*N}\cos(\psi) & 2\frac{S_\zeta^*}{M_x^*N}\cos(\psi+\frac{\pi}{2}) & 2\frac{S_\zeta^*}{M_x^*N}\cos(\psi+\pi) & 2\frac{S_\zeta^*}{M_x^*N}\cos(\psi+\frac{3\pi}{2}) & 2\zeta_x\left(\frac{\omega_x}{\Omega}\right) & 0 \\ 2\frac{S_\zeta^*}{M_y^*N}\sin(\psi) & 2\frac{S_\zeta^*}{M_y^*N}\sin(\psi+\frac{\pi}{2}) & 2\frac{S_\zeta^*}{M_y^*N}\sin(\psi+\pi) & 2\frac{S_\zeta^*}{M_y^*N}\sin(\psi+\frac{3\pi}{2}) & 0 & 2\zeta_y\left(\frac{\omega_y}{\Omega}\right) \end{bmatrix} \begin{bmatrix} \overset{*}{\zeta_1} \\ \overset{*}{\zeta_2} \\ \overset{*}{\zeta_3} \\ \overset{*}{\zeta_4} \\ \overset{*}{\bar{x}_h} \\ \overset{*}{\bar{y}_h} \end{bmatrix}$$

+

$$\begin{bmatrix} \nu_\zeta^2 & 0 & 0 & 0 & 0 & 0 \\ 0 & \nu_\zeta^2 & 0 & 0 & 0 & 0 \\ 0 & 0 & \nu_\zeta^2 & 0 & 0 & 0 \\ 0 & 0 & 0 & \nu_\zeta^2 & 0 & 0 \\ -\frac{S_\zeta^*}{M_x^*N}\sin(\psi) & -\frac{S_\zeta^*}{M_x^*N}\sin(\psi+\frac{\pi}{2}) & -\frac{S_\zeta^*}{M_x^*N}\sin(\psi+\pi) & -\frac{S_\zeta^*}{M_x^*N}\sin(\psi+\frac{3\pi}{2}) & \frac{\omega_x^2}{\Omega^2} & 0 \\ \frac{S_\zeta^*}{M_y^*N}\cos(\psi) & \frac{S_\zeta^*}{M_y^*N}\cos(\psi+\frac{\pi}{2}) & \frac{S_\zeta^*}{M_y^*N}\cos(\psi+\pi) & \frac{S_\zeta^*}{M_y^*N}\cos(\psi+\frac{3\pi}{2}) & 0 & \frac{\omega_y^2}{\Omega^2} \end{bmatrix} \begin{bmatrix} \zeta_1 \\ \zeta_2 \\ \zeta_3 \\ \zeta_4 \\ \bar{x}_h \\ \bar{y}_h \end{bmatrix} = 0 \qquad (\mathbf{1})$$

s

$$\begin{bmatrix} 1 & 0 & 0 & 0 & 0 & 0 \\ 0 & 1 & 0 & 0 & 0 & 0 \\ 0 & 0 & 1 & 0 & 0 & -S_\zeta^* \\ 0 & 0 & 0 & 1 & S_\zeta^* & 0 \\ 0 & 0 & 0 & \frac{1}{2}S_\zeta^*/M_x^* & 1 & 0 \\ 0 & 0 & -\frac{1}{2}S_\zeta^*/M_x^* & 0 & 0 & 1 \end{bmatrix} \begin{bmatrix} \overset{**}{\zeta_0} \\ \overset{**}{\zeta_2} \\ \overset{**}{\zeta_{1c}} \\ \overset{**}{\zeta_{1s}} \\ \overset{**}{\bar{x}_h} \\ \overset{**}{\bar{y}_h} \end{bmatrix}$$

+

$$\begin{bmatrix} C11 & C12 & C13 & C14 & 0 & 0 \\ C21 & C22 & C23 & C24 & 0 & 0 \\ C31 & C32 & C33 & C34 & 0 & 0 \\ C41 & C42 & C43 & C44 & 0 & 0 \\ 0 & 0 & 0 & 0 & 2\zeta_x\frac{\omega_x}{\Omega} & 0 \\ 0 & 0 & 0 & 0 & 0 & 2\zeta_y\frac{\omega_y}{\Omega} \end{bmatrix} \begin{bmatrix} \overset{*}{\zeta_0} \\ \overset{*}{\zeta_2} \\ \overset{*}{\zeta_{1c}} \\ \overset{*}{\zeta_{1s}} \\ \overset{*}{\bar{x}_h} \\ \overset{*}{\bar{y}_h} \end{bmatrix}$$

+

$$\begin{bmatrix} \nu_\zeta^2 & 0 & K13 & K14 & 0 & 0 \\ 0 & \nu_\zeta^2 & K23 & K24 & 0 & 0 \\ 0 & 0 & K33 & K34 & 0 & 0 \\ 0 & 0 & K43 & K44 & 0 & 0 \\ 0 & 0 & 0 & 0 & \frac{\omega_x^2}{\Omega^2} & 0 \\ 0 & 0 & 0 & 0 & 0 & \frac{\omega_y^2}{\Omega^2} \end{bmatrix} \begin{bmatrix} \zeta_0 \\ \zeta_2 \\ \zeta_{1c} \\ \zeta_{1s} \\ \bar{x}_h \\ \bar{y}_h \end{bmatrix} = 0 \qquad (\mathbf{2})$$

$$
\begin{aligned}
C11 &= \frac{C_\zeta}{I_\zeta \Omega}\left(1-\frac{\alpha_1}{N}\right)\\
C12 &= \frac{C_\zeta}{I_\zeta \Omega}\frac{\alpha_1}{N}\\
C13 &= -\frac{C_\zeta}{I_\zeta \Omega}\frac{\alpha_1}{N}cos\psi_1\\
C14 &= -\frac{C_\zeta}{I_\zeta \Omega}\frac{\alpha_1}{N}sin\psi_1\\
C21 &= \frac{C_\zeta}{I_\zeta \Omega}\frac{\alpha_1}{N}\\
C22 &= \frac{C_\zeta}{I_\zeta \Omega}\left(1-\frac{\alpha_1}{N}\right)\\
C23 &= \frac{C_\zeta}{I_\zeta \Omega}\frac{\alpha_1}{N}cos\psi_1\\
C24 &= \frac{C_\zeta}{I_\zeta \Omega}\frac{\alpha_1}{N}sin\psi_1\\
C31 &= -\frac{C_\zeta}{I_\zeta \Omega}\frac{2\alpha_1}{N}cos\psi_1\\
C32 &= \frac{C_\zeta}{I_\zeta \Omega}\frac{2\alpha_1}{N}cos\psi_1\\
C33 &= \frac{C_\zeta}{I_\zeta \Omega}\left(1-\frac{\alpha_1}{N}\right)-\frac{C_\zeta}{I_\zeta \Omega}\frac{\alpha_1}{N}cos2\psi_1\\
C34 &= 2-\frac{C_\zeta}{I_\zeta \Omega}\frac{\alpha_1}{N}sin2\psi_1\\
C41 &= \frac{C_\zeta}{I_\zeta \Omega}\frac{2\alpha_1}{N}sin\psi_1\\
C42 &= -\frac{C_\zeta}{I_\zeta \Omega}\frac{2\alpha_1}{N}sin\psi_1\\
C43 &= -2-\frac{C_\zeta}{I_\zeta \Omega}\frac{\alpha_1}{N}sin2\psi_1\\
C44 &= \frac{C_\zeta}{I_\zeta \Omega}\left(1-\frac{\alpha_1}{N}\right)+\frac{C_\zeta}{I_\zeta \Omega}\frac{\alpha_1}{N}cos2\psi_1
\end{aligned}
\qquad (\mathbf{3})
$$

$$
\begin{aligned}
K13 &= \frac{C_\zeta}{I_\zeta \Omega}\frac{\alpha_1}{N}sin\psi_1\\
K14 &= -\frac{C_\zeta}{I_\zeta \Omega}\frac{\alpha_1}{N}cos\psi_1\\
K14 &= -\frac{C_\zeta}{I_\zeta \Omega}\frac{\alpha_1}{N}cos\psi_1\\
K23 &= -\frac{C_\zeta}{I_\zeta \Omega}\frac{\alpha_1}{N}sin\psi_1\\
K24 &= \frac{C_\zeta}{I_\zeta \Omega}\frac{\alpha_1}{N}cos\psi_1\\
K33 &= \nu_\zeta^2-1-\frac{C_\zeta}{I_\zeta \Omega}\frac{\alpha_1}{N}sin2\psi_1\\
K34 &= \frac{C_\zeta}{I_\zeta \Omega}\left(1-\frac{\alpha_1}{N}\right)-\frac{C_\zeta}{I_\zeta \Omega}\frac{\alpha_1}{N}cos2\psi_1\\
K43 &= -\frac{C_\zeta}{I_\zeta \Omega}\left(1-\frac{\alpha_1}{N}\right)-\frac{C_\zeta}{I_\zeta \Omega}\frac{\alpha_1}{N}cos2\psi_1\\
K44 &= \nu_\zeta^2-1-\frac{C_\zeta}{I_\zeta \Omega}\frac{\alpha_1}{N}sin2\psi_1
\end{aligned}
\qquad (\mathbf{4})
$$

$$
\begin{aligned}
C11 &= \frac{C_\zeta}{I_\zeta \Omega}\left(1-\frac{\alpha_1}{N}\right)\\
C12 &= \frac{C_\zeta}{I_\zeta \Omega}\frac{\alpha_1}{N}\\
C21 &= \frac{C_\zeta}{I_\zeta \Omega}\frac{\alpha_1}{N}\\
C22 &= \frac{C_\zeta}{I_\zeta \Omega}\left(1-\frac{\alpha_1}{N}\right)\\
C33 &= \frac{C_\zeta}{I_\zeta \Omega}\left(1-\frac{\alpha_1}{N}\right)\\
C44 &= \frac{C_\zeta}{I_\zeta \Omega}\left(1-\frac{\alpha_1}{N}\right)
\end{aligned}
\qquad (\mathbf{5})
$$

$$
\begin{aligned}
K33 &= \nu_\zeta^2-1\\
K34 &= \frac{C_\zeta}{I_\zeta \Omega}\left(1-\frac{\alpha_1}{N}\right)\\
K43 &= -\frac{C_\zeta}{I_\zeta \Omega}\left(1-\frac{\alpha_1}{N}\right)\\
K44 &= \nu_\zeta^2-1
\end{aligned}
\qquad (\mathbf{6})
$$

Even without body motion, the equations contain periodic terms when damper degradation is present ($\alpha_1 \neq 0$). Using Floquet Transition Matrix theory results in decay rate predictions (not shown in the paper) similar to those seen in Fig. 6. For $\alpha_1 = 0$ (no damper 1 degradation), four modes with equal decay rate at the same levels as in Fig. 6 are observed. For increasing levels of degradation, three modes remain unchanged whereas the decay rate of the fourth mode reduces, similar to what was seen in Fig. 6.

With the body motions included ($\bar{x} \neq 0$, $\bar{y} \neq 0$) and the rotor lag motions still represented using multi-blade coordinates (Eq. 2), Floquet Transition Matrix theory was used to evaluate the coupled system stability characteristics, and the modal decay rate for the lowest damped mode is presented in Fig. 8 for increasing levels of degradation. These results mirror the predictions in Fig. 7, where the rotor motions were represented in individual blade coordinates.

In the classical Coleman-Feingold ground resonance analysis, which considers identical blades/dampers and represents the rotor lag motions in multi-blade coordinates (Refs. 1 – 3), the equations have constant coefficients and the stability characteristics can conveniently be evaluated by solving an eigenvalue problem. Although degradation in damper 1 introduces periodic terms in the rotor-body equations (Eq. 2), as noted in the Analysis section, a constant coefficient approximation could still be applied, followed by the solution of an eigenvalue problem, instead of employing Floquet Transition Matrix theory. Such an approach is frequently taken for rotor aeroelastic stability analysis in forward flight (Refs. 2, 3) with the constant coefficient approximation applied to the periodic terms in the linearized equations, and the stability predictions generally compare well with those from Floquet Transition matrix theory at low to moderate advance ratios. Figure 9 shows the stability predictions from an eigenvalue analysis following the application of the constant coefficient approximation to Eq. 2 (with matrix terms in Eq. 5 and 6). The damping levels predicted are higher than observed in Fig. 8, especially for higher levels of degradation. Figure 10 shows the minimum damping (at the bottom of the "resonance bucket" in Figs. 7–9), as a function of degradation level (α_1). With the constant coefficient approximation, the reduction in damping varies linearly with level of degradation. Using Floquet Transition Matrix theory to properly account for the periodic terms in the system when damper degradation is present results in lower damping predictions, with the difference from the constant coefficient results increasing progressively with increasing α_1. In Fig. 10, at 20% damper degradation (α_1=0.2), the loss in damping predicted using constant coefficient approximation is 85% of the loss in damping from Floquet theory. In comparison, at 50% and 100% damper degradation (α_1=0.5 and 1), the predicted loss in damping with the constant coefficient approximation is 66% and 46% respectively of the Floquet predictions.

In the classical Coleman-Feingold ground resonance analysis with identical blades/dampers and rotor lag motions in multi-blade coordinates, only the rotor cyclic lag motions (ζ_{1c} and ζ_{1s}) and fuselage motions ($\bar{x}$ and $\bar{y}$) are retained, and the rotor collective and differential lag motions (ζ_o and ζ_2) have no participation. Eliminating collective and differential lag motions in Eq. 2 (by removal of first two rows and columns) the system stability was reanalyzed using Floquet theory. It should be noted that when damper 1 degradation is introduced, even after the removal of collective and differential lag motions, periodic terms will still be present in Eq. 2, specifically in the C33, C34, C43 and C44 terms in the damping matrix and the K33, K34, K43 and K44 terms in the stiffness matrix. The stability characteristics with the removal of the collective and differential motions is shown in Fig. 11. A significant over-prediction of damping levels is observed, relative to damping predictions when all the rotor lag modes are included. In fact, the damping predictions with the collective and differential modes eliminated are very similar to those previously seen in Fig. 10 using a constant coefficient approximation. From the above it is clear that when there is degradation or failure in a lag damper, it is critical to retain the collective and differential lag modes (along with the cyclic lag modes) when analyzing ground resonance, and eliminating these modes, as is done in a classical Coleman-Feingold ground resonance analysis, would lead to erroneous predictions of stability levels.

When using multi-blade coordinates, although the constant coefficient approximation over-predicts the damping levels when there is damper degradation/failure (Fig. 10), it is nevertheless interesting to delve deeper. To do so, the fuselage motion is suppressed ($\bar{x}$=0, $\bar{y}$=0), and after eliminating the last two rows and columns in the matrices in Eq. 2, the constant coefficient approximation is again applied and the eigenvalue problem is solved. Figure 12 shows the modal frequencies with 50% damper 1 degradation (α_1=0.5), and Figs. 13 and 14, respectively, show the modal decay rates corresponding to 50% damper 1 degradation, and complete damper 1 failure (α_1= 1). The modal frequencies in Fig. 12 are unchanged from the case when there is no damage (α_1=0), and the collective/differential lag modes, the progressing and regressing modes are clearly identified. However, while the collective and differential modes for the undamaged case were decoupled, the two modes are completely coupled here (determined through the examination of the eigenvectors). In fact, one of the coupled modes is $\zeta_o+\zeta_2$ and the other is $\zeta_o-\zeta_2$, as shown in Fig. 15. In the decay rate plots (Figs. 13 and 14) the decay rate of one of the coupled collective/differential modes is seen to remain unchanged from the level for all the modes when there is no damper damage/degradation. The decay rates for the progressing and regressing modes are identical and show a reduction. Finally, the decay rates of the other coupled collective/differential mode show twice the reduction seen in the progressing/regressing modes. One of the coupled collective/differential modes shown in Fig. 15 contains the damaged blade, and the other one does not. The mode with the highest damping in Figs. 13 and 14, unchanged from a healthy rotor, is the coupled collective/differential mode that does not include the blade with the damaged damper, and the mode with the lowest damping is the coupled

collective/differential mode that includes the blade with the damaged damper.

HINGELESS ROTOR SUMMARY OF RESULTS

A study similar to the one in the previous section was conducted after switching from the articulated rotor to a hingeless main rotor (with a non-dimensional rotating lag frequency of 0.65/rev at a 300 RPM rotational speed). Figure 16 shows the reduction in system damping with increasing levels of degradation in damper 1. The results in Fig. 16 are based on a Floquet analysis of the coupled rotor-body system with rotor lag motions in multi-blade coordinates (Eq. 2), but very similar results are obtained when the Floquet analysis is conducted using individual blade coordinates to represent the blade lag motions (Eq. 1). Figure 17 shows the minimum damping at resonance condition versus damper degradation level. As with the articulated rotor in Fig. 10, the constant coefficient approximation (applied with rotor lag motions in multi-blade coordinates) predicts higher levels of damping than the Floquet analysis. The reduction in damping using the constant coefficient approximation at 20%, 50%, and 100% degradation is 89%, 74%, and 55% of that from the Floquet analysis. Observations made for the articulated rotor on the importance of the inclusion of the collective and differential lag modes in the ground resonance analysis apply equally to the hingeless rotor. Similarly, the coupling of the collective and differential modes reported for the articulated rotor was observed for the hingeless rotor, as well.

CONCLUSIONS

This paper examines ground resonance behavior for a helicopter with a 4-bladed articulated and a soft in-plane hingeless rotor, when one of the lag dampers is degraded or has even failed entirely. Three different analysis methods are used: (1) the lag motions/equations are represented using rotating-frame individual blade coordinates, and solved using Floquet theory, (2) the lag motions/equations are transformed to multi-blade coordinates, but still solved using Floquet theory since periodic terms are present when there is degradation in one of the dampers, and (3) with the lag motions/equations in multi-blade coordinates, the constant coefficient approximation is applied and an eigen-analysis is conducted to evaluate the system stability. From the results presented the following observations could be made:

1. Regardless of whether the blade lag motions are represented in individual blade coordinates or multi-blade coordinates, the predicted stability levels are identical if the analysis is conducted using Floquet theory.
2. If the lag motions and equations are in multi-blade coordinates, collective and differential lag needs to be retained (unlike the case of a classical ground resonance analysis where only the cyclic lag modes and body motions are required).
3. If the lag motions and equations are in multi-blade coordinates, applying the coefficient approximation is equivalent to smearing the total loss in damping in a single damper equally over all the dampers. The predicted loss in system damping is smaller than that from a Floquet analysis, and the differences are greater for larger levels of damper degradation. For the articulated rotor, at 20% degradation, the predicted loss in damping using the constant coefficient approximation was 85% of that with Floquet theory, but at 50% and 100% damper degradation the predicted loss in damping with the constant coefficient approximation is 66% and 46% of that with Floquet theory. For the hingeless rotor, reduction in damping using the constant coefficient approximation at 20%, 50%, and 100% degradation is 89%, 74%, and 55% of that from Floquet theory.
4. Considering only the rotor (no fuselage) in multi-blade coordinates, when Floquet theory is used the decay rate of a single mode drops proportionate to the degradation in the single damper, while the other modes are unaffected. In comparison, if the constant coefficient approximation is used, only one of the modes is unaffected (specifically one of the coupled collective/differential modes), the progressing and regressing modes show some reduction in damping, and the second coupled collective/differential mode shows twice the reduction in damping.

Future studies will extend to 3- and 5-bladed rotors. In particular, we anticipate that for 5-bladed rotors, in addition to the collective lag mode the 2c and 2s modes will need to be retained as well.

ACKNOWLEDGMENTS

The second author gratefully acknowledges the many enjoyable and enriching discussions with Dr. Kenneth Rosen (retired VP Engineering, Sikorsky Aircraft Corp). This study developed as a result of such discussions.

REFERENCES

1. Coleman, R. P., and Feingold, A. M., "Theory of self-excited mechanical oscillations of helicopter rotors with hinged blades," NACA-TR-1351, Jan 1, 1958.
2. Johnson, W., "Helicopter Theory," Dover Publications, 1994.
3. Johnson, W., "Rotorcraft Aeromechanics," Cambridge University Press, 2013.
4. Bousman,W. G., "An Experimental Investigation of the Effects of Aeroelastic Couplings on Aeromechanical Stability of a Hingeless Rotor Helicopter," *Journal of the American Helicopter Society*, Vol. 26, No. 1, 1981, pp. 46–54.
5. Ormiston, R. A., "Investigations of Hingeless Rotor Stability," *Vertica*, Vol. 7, No. 2, 1983, pp. 143–181.
6. Bousman, W. G., "The Effects of Structural Flap-Lag and Pitch-Lag Coupling on Soft Inplane Hingeless Rotor Stability in Hover," NASA TP 3002, May 1990.
7. Zotto, M. D., and Loewy, R. G., "Influence of Pitch-Lag Coupling on Damping Requirements to Stabilize

Ground/Air Resonance," *Journal of the American Helicopter Society*, Vol. 37, No. 4, 1992, pp. 68–71.
8. Gandhi, F., and Hathaway, E., "Optimized Aeroelastic Couplings for Alleviation of Helicopter Ground Resonance," *Journal of Aircraft*, Vol. 35, No. 4, 1998, pp. 582–589.
9. Hathaway, E., and Gandhi, F., "Concurrently Optimized Aeroelastic Couplings and Rotor Stiffness for Alleviation of Helicopter Aeromechanical Instability, *J. of Aircraft*, Vol. 38, No. 1, Jan–Feb 2001.
10. Takahashi, M. D., and Friedmann, P. P., "Active Control of Helicopter Air Resonance in Hover and Forward Flight," *AIAA-88-2407*. https://doi.org/10.2514/6.1988-2407
11. Gandhi, F., and Weller, W., "Active Aeromechanical Stability Augmentation using Fuselage State Feedback," *Proc. of the 53rd Annual Forum of the American Helicopter Society*, Virginia Beach, Virginia, April 1997, pp. 1350 – 1362.
12. Hathaway, E., and Gandhi, F., "Individual Blade Control for Alleviation of Helicopter Ground Resonance," *Proc. of the 39th AIAA/ASME/ASCE/AHS/ASC Structures, Structural Dynamics and Materials Conference*, Long Beach, California, April 1998, pp. 2507-2517, AIAA Paper No. 98-2006.
13. Prasanth, R., Mehra, R., and Bennett, R., "Active Control of Aeromechanical Instability," AIAA-99-42222. https://doi.org/10.2514/6.1999-4222.
14. Cardin, V., "Practical Examples of New Technologies in Dynamics as Applied to Eurocopter Products," *Proc. of the 56th Annual Forum of the American Helicopter Society*, Alexandria, VA, May 2000.
15. Hammond, C. E., "An Application of Floquet Theory to Prediction of Mechanical Instability," *J. of the American Helicopter Society*, Vol. 19, No. 4, Oct 1974, pp. 14-23(10). DOI: https://doi.org/10.4050/JAHS.19.14.
16. Peters, D. A., and Hohenemser, K. H., "Application of Floquet Transition Matrix Theory to Problems of Lifting Rotor Stability," *J. of the American Helicopter Society*, Vol. 17, No. 3, July 1972, pp. 3-12.

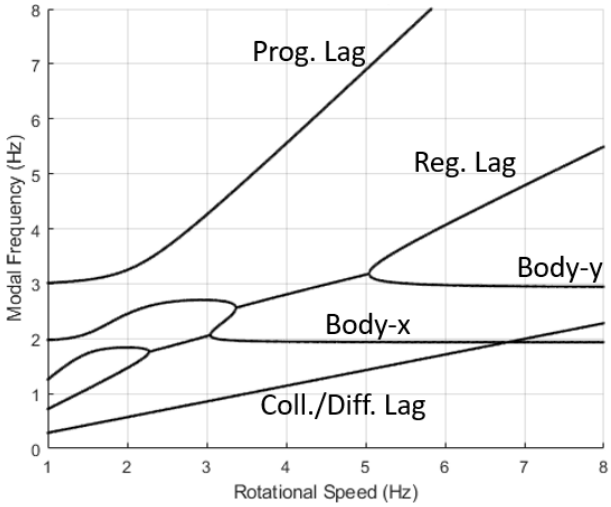

Fig. 1: Articulated rotor-body modal frequencies (C_ζ, ζ_x, ζ_y =0)

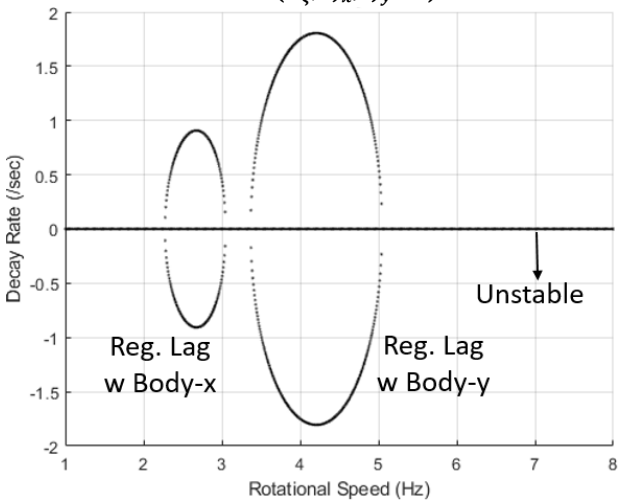

Fig. 2: Articulated rotor-body modal damping (C_ζ, ζ_x, ζ_y =0)

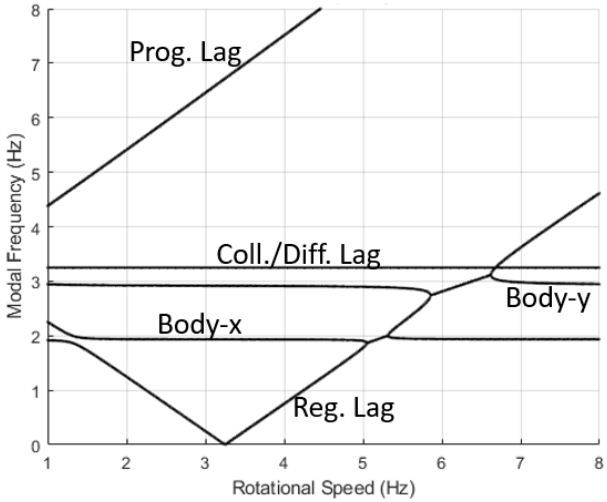

Fig. 3: Hingeless rotor-body modal frequencies (C_ζ, ζ_x, ζ_y =0)

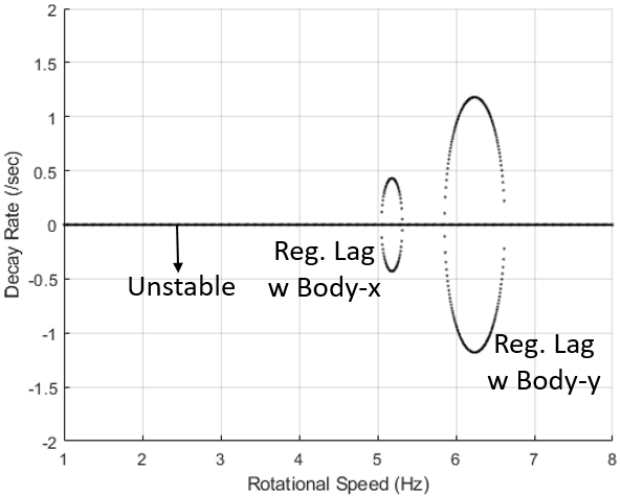

Fig. 4: Hingeless rotor-body modal damping (C_ζ, ζ_x, ζ_y =0)

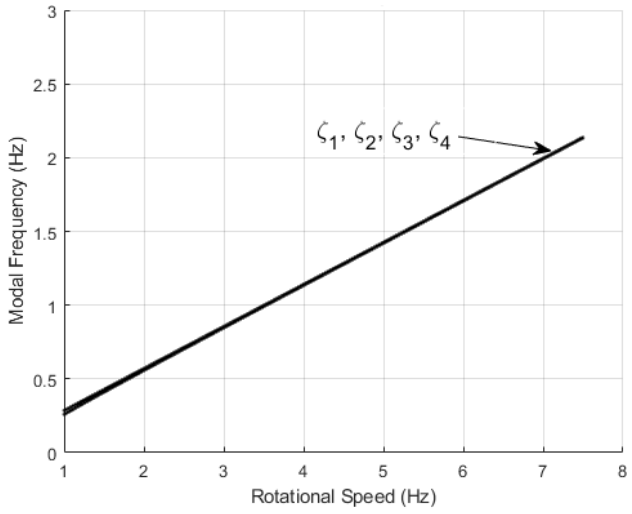

Fig. 5: Articulated rotor-only modal frequencies (individual blade coordinates)

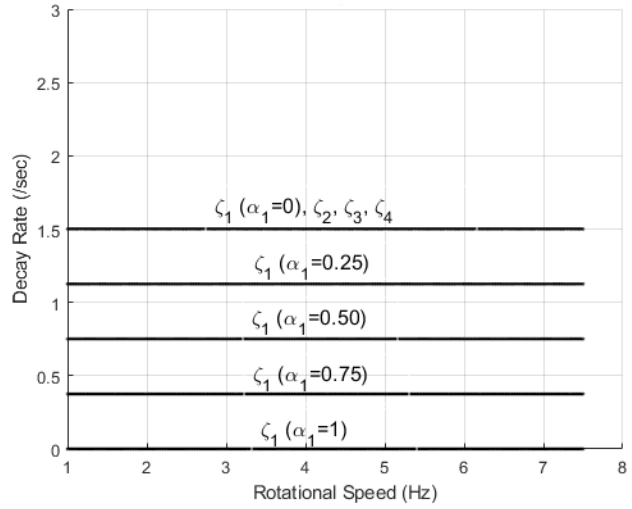

Fig. 6: Articulated rotor-only modal damping from Floquet theory (individual blade coordinates) for healthy and degraded damper

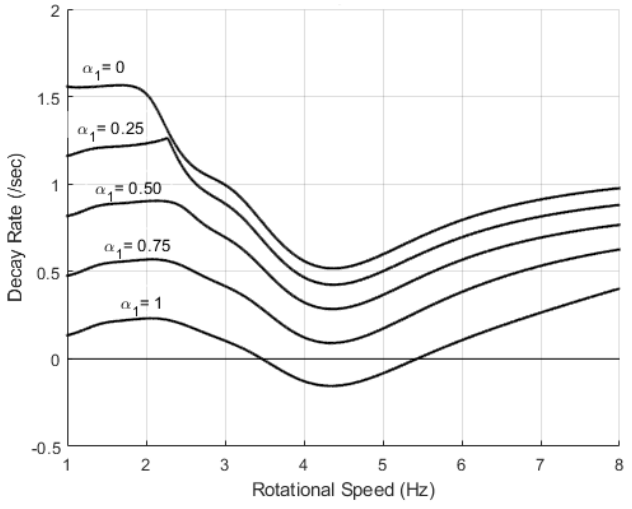

Fig. 7: Articulated rotor-body modal damping from Floquet theory (lowest damped mode, individual blade coordinates) with increasing damper degradation

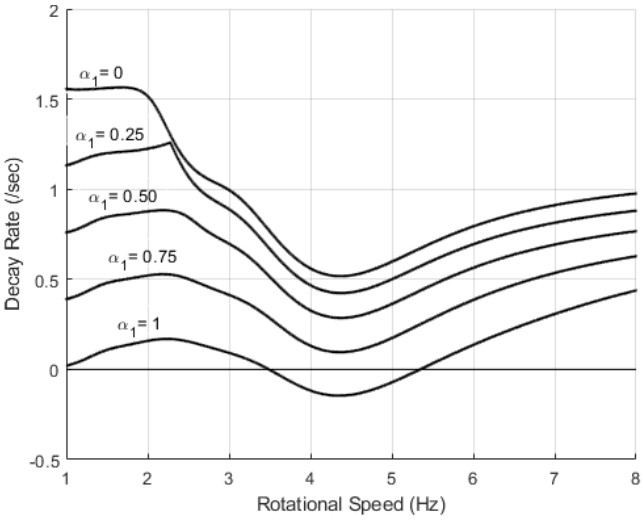

Fig. 8: Articulated rotor-body modal damping from Floquet theory (lowest damped mode, multi-blade coordinates) with increasing damper degradation

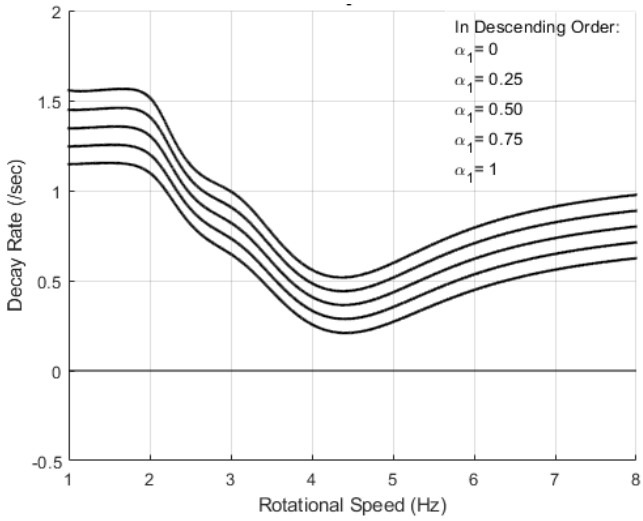

Fig. 9: Articulated rotor-body modal damping from eigen-analysis (lowest damped mode, multi-blade coordinates) with increasing damper degradation

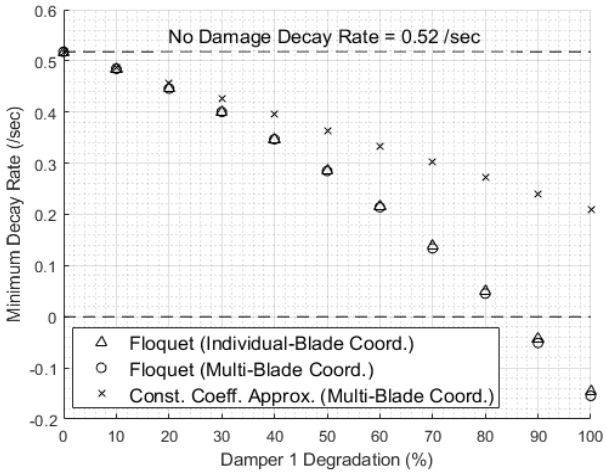

Fig. 10: Articulated rotor ground resonance stability comparisons for increasing levels of degradation

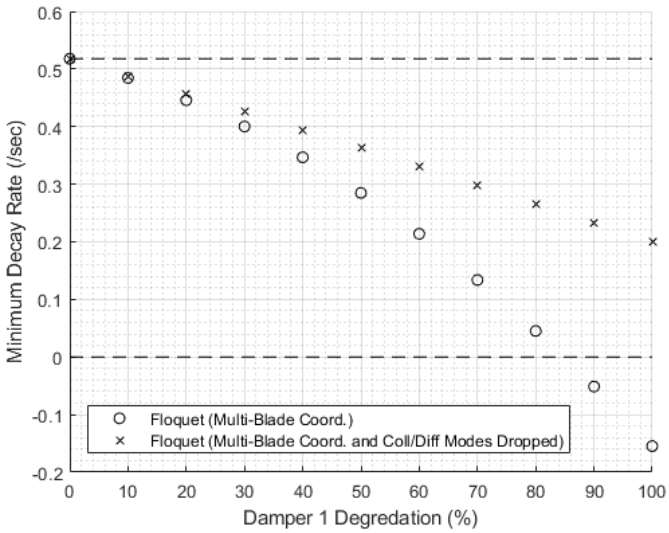

Fig. 11: Articulated rotor ground resonance stability comparisons, with and without coll./diff. lag modes

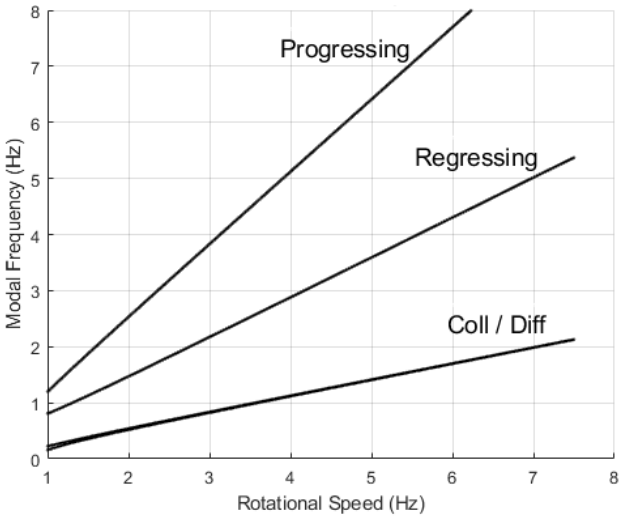

Fig. 12: Articulated rotor-only modal frequencies (multi-blade coordinates)

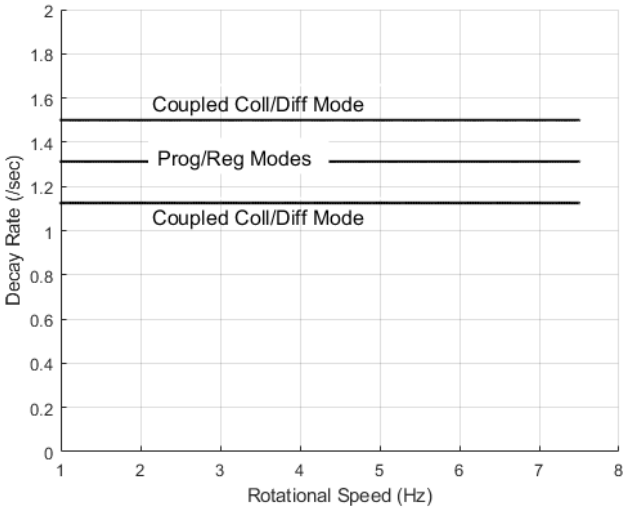

Fig. 13: Articulated rotor-only modal damping (multi-blade coordinates). Results from constant coefficient approximation and eigen-analysis (50% degradation)

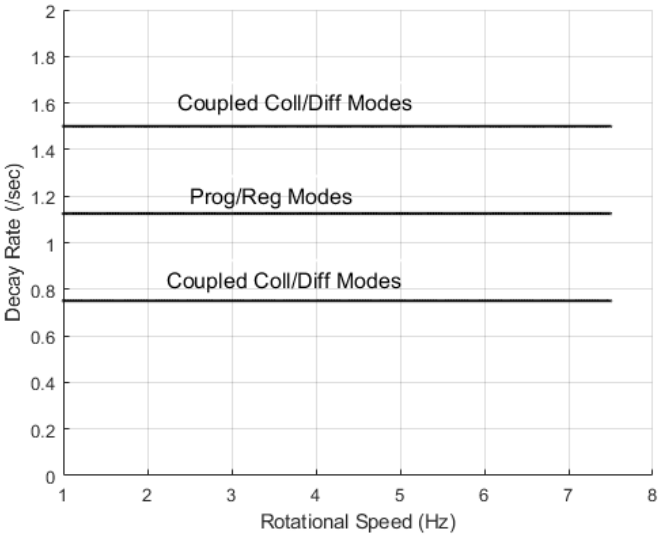

Fig. 14: Articulated rotor-only modal damping (multi-blade coordinates). Results from constant coefficient approximation and eigen-analysis (100% degradation)

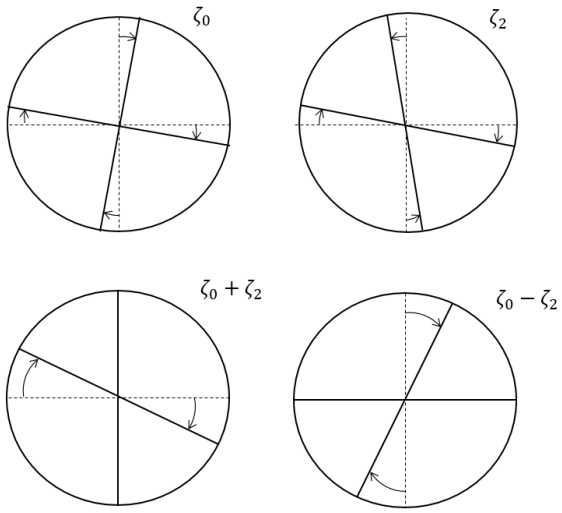

Fig. 15: Rotor-only coupled coll./diff. lag modes

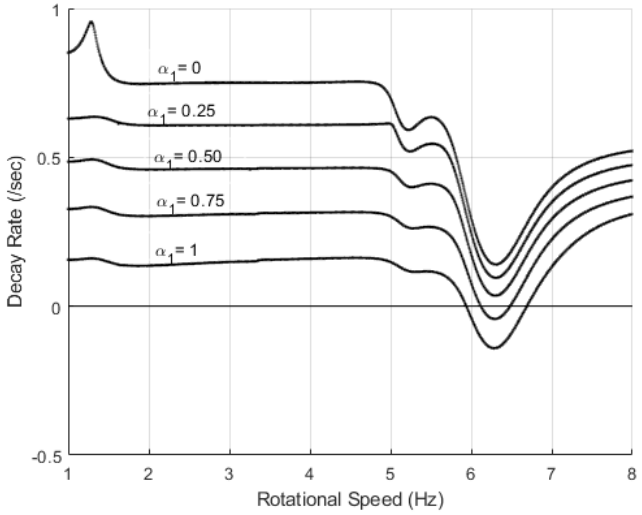

Fig. 16: Hingeless rotor-body modal damping from Floquet theory (lowest damped mode, multi-blade coordinates) with increasing damper degradation

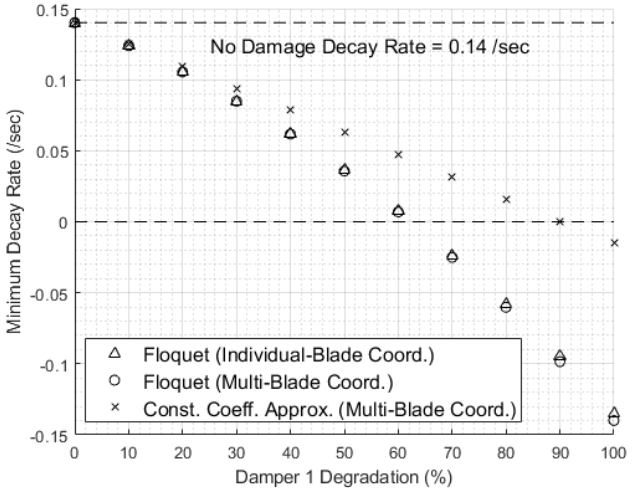

Fig. 17: Hingeless rotor ground resonance stability comparisons for increasing levels of degradation

Table 1: System Rotor-Body Parameters

Quantity	Description	Value
$\boldsymbol{S_\zeta^* = \frac{S_\zeta R}{I_\zeta}}$	$\boldsymbol{S_\zeta}$: First blade lag mom. of inertia $\boldsymbol{I_\zeta}$: Second blade lag mom. of inertia $\boldsymbol{R}$: Rotor Radius	$\frac{3}{2}$
$\boldsymbol{M_x^* = \frac{(M_x + NM_b)R^2}{NI_\zeta}}$	$\boldsymbol{(M_x + NM_b)}$: Support and blade mass in x-direction	68.175
$\boldsymbol{M_y^* = \frac{(M_y + NM_b)R^2}{NI_\zeta}}$	$\boldsymbol{(M_y + NM_b)}$: Support and blade mass in y-direction	29.708
$\boldsymbol{\omega_x = \frac{k_x}{M_x + NM_b}}$	Support Frequency in x-direction k_x: Support stiffness in x-direction	12.148 rad/sec
$\boldsymbol{\omega_y = \frac{k_y}{M_x + NM_b}}$	Support Frequency in y-direction k_y: Support stiffness in y-direction	18.402 rad/sec
$\boldsymbol{\nu_\zeta}$	Non-dimensional rotating lag natural freq.	0.285/rev (articulated) 0.65/rev at 5Hz* (hingeless)

*$\nu_\zeta = 0.65\left(\frac{5}{\Omega}\right)$ (Ω in Hz)

Table 2: System Damping Parameters

Quantity	Description	Value
$\boldsymbol{\zeta_x}$	Modal Damping Ratio for support motion in x-direction	0.30 (articulated) 0.15 (hingeless)
$\boldsymbol{\zeta_y}$	Modal Damping Ratio for support motion in y-direction	
$\boldsymbol{C_\zeta / I_\zeta}$	Ratio of rotor lag damping coeff. to blade lag inertia	3.0 (articulated) 1.5 (hingeless)